# SUPPLEMENTARY MATERIAL

## Alpha and Theta Mechanisms Operating in Internal-External Attention Competition

### S1. Assignment of source space voxels to the selected ROIs

In the LORETA-KEY software, each of the 6239 voxels is provided with its x,y,z MNI coordinates, and with the lobe, region and Brodmann area the voxel belongs to. Therefore, the assignment of a voxel to a ROI was based on the label specifying its region (in our study: Lingual Gyrus (LG), Cuneus (CU), Inferior Temporal Gyrus (ITG), Middle Frontal Gyrus (MFG), Anterior Cingulate (ACC), Precuneus (PCU)). The assignment of a voxel to the left, right or medial part of a ROI was based on the x coordinate provided by LORETA-KEY software; the x coordinate is directed from left to right, with 5 mm resolution, and assumes negative values for voxel in the left hemisphere and positive values for voxel in the right hemisphere (the origin of MNI coordinate system is located at the anterior commissure). Specifically, we performed the following assignment: voxels belonging to a region (e.g. CU or LG) were assigned to the left part of that ROI (i.e. $LGCU_L$) if they have $x < -5$ mm, to the right part of that ROI ($LGCU_R$) if they have $x > +5$ mm and to the medial part of that ROI ($LGCU_M$) if they have $-5 \text{ mm} \leq x \leq +5$ mm. Some ROIs do not have the medial part (ITG and MFG). In our study, for the ROIs ACC and PCU we considered only the medial part (hence, we did not use the subscript). Indeed, the Anterior Cingulate region lies mostly medially and only a few left and right voxels remained excluded. On the contrary the overall Precuneus region extends also superiorly on the left and right even beyond the LGCU region; however, we preferred to maintain the selection limited to the medial portion (see Figure 1) since the results motivating its selection (voxel-wise statistical analysis contrasting ExtAtt vs Rest in Theta Band, see Figure 5) suggested that the medial part was mainly involved. The Supplementary Table 1 provides the number of voxels for each investigated ROI.

**S2. Selection of model order for the bivariate autoregressive (BVAR) models of the data in the computation of spectral Granger Causality**

We did not use the Akaike Information Criterion to identify the model order for the AR model in this study, since in some preliminary tests we found that the minimum of this criterion often settled to low values of the model order far to reproduce the data well (a problem already observed previously, see for example (Wang et al. 2016)). Hence, to select the model order, we compared the power spectral estimates obtained by the BVAR models and those estimated directly from the temporal ROIs waveform via the Welch's method. This was done for different model orders (from 5 to 45 with step of 5) and the mean squared difference between the two estimates was computed (within the range 3-20 Hz) and averaged across the ROIs and participants. We maintained separated the assessment for the frontal-temporal ROIs (ACC, $MFG_L$, $MFG_R$, $ITG_L$, $ITG_R$) and for the posterior ROIs (PCU, $LGCU_L$, $LGCU_M$, $LGCU_R$) since the error showed a different rate of decrease in the two sets of ROIs, as shown in the Supplementary Figure 1. These results show that at model order 30, both errors settled at a lower saturation level. Actually, the error for the posterior ROIs reached the saturation level before (at model order 20) and then fluctuated around it; however, using smaller value for the model order (e.g. 25) caused the AR model to missed the theta peak in the frontal ROIs (see Supplementary Figure 2). For completeness, Supplementary Figures from 2 to 10 showed, for each selected ROI, the PSDs estimated directly on the actual ROI signals (Panel A) and the comparison between them and those obtained from the AR models with model order 30 (Panel B). Results in all panels are averaged across the participants.

**S3. Results of the voxel-wise statistical analysis**

Supplementary Tables 2-4 refer to the results of the voxel-wise statistical analysis as to the theta band (see Figure 5) while Supplementary Tables 5-6 as to the alpha band (see Figure 6). For each statistical comparison, the table reports: the regions the voxels statistically significant belong too (based on the region label provided for each voxel in the software LORETA-KEY), the number of statistically significant voxel in each region (distinguishing between the left, right, medial subdivision as described in Supplementary Section S1) and the largest value of the observed t-statistic on the whole region (irrespective of the side). It is worth noticing that these comparisons are one-tailed. Comparisons in the other direction did not provide any significance.

**Supplementary Table 1**: Number of voxels for each investigated ROI according to the procedure of voxel assignment described in Supplementary section S1.

| ***ROI*** | ***number of voxels*** |
|---|---|
| $LGCU_L$ | 158 |
| $LGCU_M$ | 142 |
| $LGCU_R$ | 157 |
| PCU | 122 |
| $ITG_L$ | 78 |
| $ITG_R$ | 73 |
| $MFG_L$ | 237 |
| $MFG_R$ | 245 |
| ACC | 100 |

**Supplementary Table 2**: Results of the voxel-wise statistical analysis comparing the theta power between ExtAtt vs Rest (ExtAtt > Rest)

| **Region** | **n. voxels: L/M/R** | **t-statics on the ROI** |
|---|---|---|
| Cingulate Gyrus | 7/21/5 | 5.06 |
| Cuneus | 12/10/5 | 4.82 |
| Fusiform Gyrus | 0/-/6 | 3.44 |
| Lingual Gyrus | 30/19/44 | 4.62 |
| Middle Occipital Gyrus | 2/-/0 | 3.38 |
| Parahippocampal | 4/-/4 | 4.03 |
| Posterior Cingulate | 18/47/15 | 5.36 |
| Precuneus | 34/34/22 | 5.52 |

**Supplementary Table 3**: Results of the voxel-wise statistical analysis comparing the theta power between IntAtt vs Rest (IntAtt > Rest)

| **Region** | **n. voxels: L/M/R** | **t-statics on the ROI** |
|---|---|---|
| Anterior Cingulate | 15/69/4 | 3.18 |
| Cingulate Gyrus | 8/21/4 | 2.69 |
| Inferior Frontal Gyrus | 122/-/0 | 3.18 |
| Insula | 17/-/0 | 3.41 |
| Medial Frontal Gyrus | 19/28/1 | 2.85 |
| Middle Frontal Fyrus | 42/-/0 | 3.04 |
| Orbital Gyrus | 6/-/0 | 2.57 |
| Parahippocampal Gyrus | 14/-/0 | 3.06 |
| Rectal Gyrus | 9/3/0 | 2.76 |
| Subcallosal Gyrus | 8/8/0 | 3.09 |
| Superior Frontal | 5/1/0 | 2.52 |
| Superior Temporal Gyrus | 39/-/0 | 2.84 |

**Supplementary Table 4**: Results of the voxel-wise statistical analysis comparing the theta power between IntExtAtt vs Rest (IntExtAtt > Rest)

| **Region** | **n. voxels: L/M/R** | **t-statics on the ROI** |
|---|---|---|
| Anterior Cingulate | 0/2/1 | 3.05 |
| Cingulate Gyrus | 2/0/0 | 3.46 |
| Cuneus | 10/0/0 | 3.25 |
| Fusiform Gyrus | 93/-/65 | 3.39 |
| Inferior Frontal Gyrus | 1/-/5 | 3.02 |
| Inferior Parietal Gyrus | 0/-/4 | 2.91 |
| Inferior Temporal Gyrus | 61/-/33 | 3.44 |
| Insula | 10/-/11 | 3.48 |
| Lingual Gyrus | 9/0/0 | 3.14 |
| Medial Frontal Gyrus | 0/7/5 | 3.06 |
| Middle Occipital | 27/-/9 | 3.48 |
| Middle Temporal Gyrus | 99/-/18 | 3.62 |
| Parahippocampal | 77/-/75 | 3.61 |
| Postcentral Gyrus | 2/-/9 | 3.43 |
| Posterior Cingulate | 19/1/0 | 3.49 |
| Precentral Gyrus | 2/-/19 | 3.27 |
| Precuneus | 25/3/0 | 3.57 |
| Superior Frontal Gyrus | 0/2/5 | 3.02 |
| Superior Temporal Gyrus | 54/-/5 | 3.19 |

**Supplementary Table 5**: Results of the voxel-wise statistical analysis comparing the alpha power between ExtAtt vs Rest (ExtAtt < Rest)

| **Region** | **n. voxels: L/M/R** | **t-statics on the ROI** |
|---|---|---|
| Angular Gyrus | 15/-/0 | -3.15 |
| Cingulate Gyrus | 9/41/18 | -3.17 |
| Cuneus | 89/87/91 | -3.33 |
| Fusiform Gyrus | 111/-/99 | -3.68 |
| Inferior Occipital Gyrus | 17/-/19 | -3.26 |
| Inferior Parietal Gyrus | 7/-/136 | -3.35 |
| Inferior Temporal Gyrus | 63/-/37 | -3.73 |
| Insula | 5/-/38 | -3.35 |
| Lingual Gyrus | 68/43/65 | -3.37 |
| Middle Occipital Gyrus | 74/-/67 | -3.66 |
| Middle Temporal Gyrus | 103/-/113 | -3.75 |
| Parahippocampal Gyrus | 89/-/90 | -3.76 |
| Postcentral Gyrus | 2/3/119 | -3.05 |
| Posterior Cingulate | 19/40/19 | -3.27 |
| Precuneus | 104/108/120 | -3.24 |
| Superior Occipital Gyrus | 8/-/9 | -3.21 |
| Superior Parietal Lobule | 30/2/65 | -3.1 |
| Superior Temporal Gyrus | 39/-/95 | -3.72 |
| Supramarginal Gyrus | 10/-/24 | -3.47 |

**Supplementary Table 6**: Results of the voxel-wise statistical analysis comparing the alpha power between IntExtAtt vs Rest (IntExtAtt < Rest)

| **Region** | **n. voxels: L/M/R** | **t-statics on the ROI** |
|---|---|---|
| Inferior Parietal Gyrus | 0/-/20 | -3.06 |
| Superior Parietal Lobule | 0/-/2 | -3 |

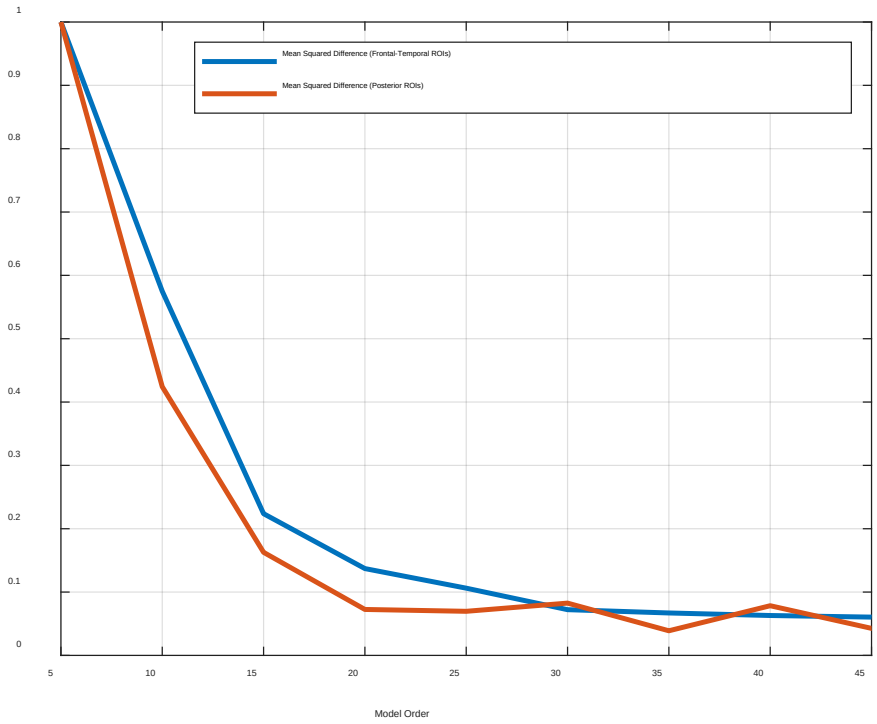


## Supplementary Figure 1

**Supplementary Figure 1** – Mean squared difference (error) between the PSDs estimated directly on the actual ROIs data and those obtained by the BVAR models. The model order was increased from 5 to 45 with step of 5. The represented error values were obtained in the frequency range 3-20 Hz and averaged across all ROIs (in the two sets, fronto-temporal and posterior) and participants; furthermore for clarity of visualization, they were normalized with respect to the maximum error value (at model order 5).

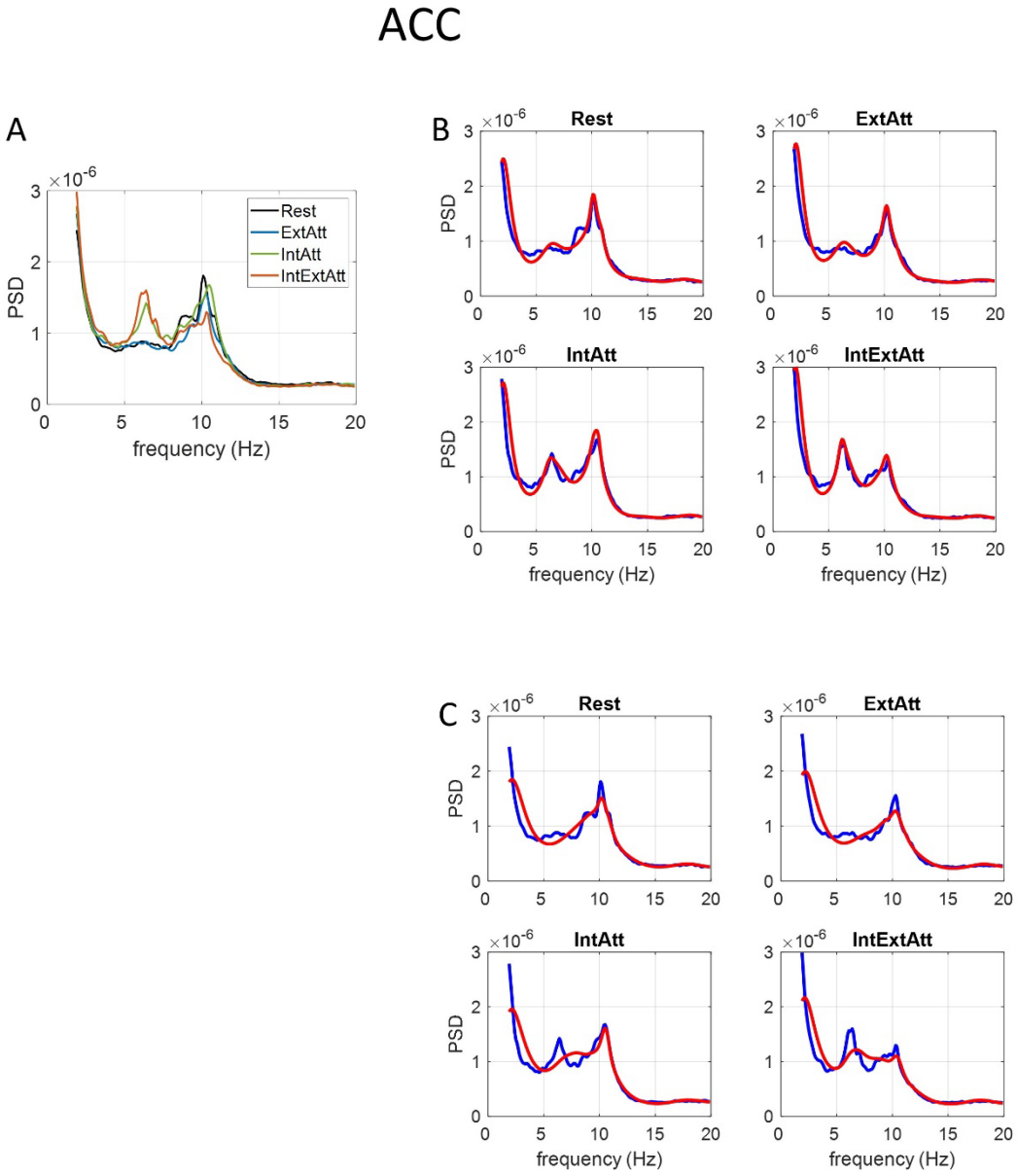


**Supplementary Figure 2**

**Supplementary Figure 2 – Panel A**: PSDs estimated directly on the ROI (ACC) signal in the four conditions (Rest, ExtAtt, IntAtt, IntExtAtt). **Panel B** – Comparison between the PSD estimated directly on the ROI signal (blue lines, the same curves as in Panel A) and the PSD obtained from the AR model of the ROI signal using model order 30 (red lines). **Panel C**–The same as in Panel B but using model order 25, showing that the theta peak was not well reproduced by the AR model. Values are in $(\mu A/mm^2)^2/Hz$.

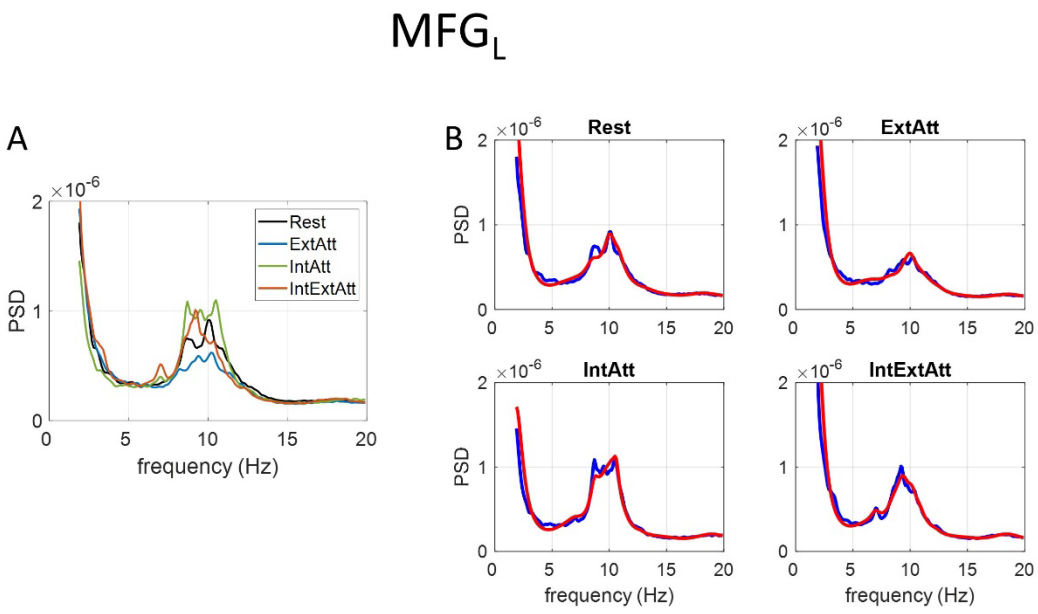


**Supplementary Figure 3**

**Supplementary Figure 3 - Panel A**: PSDs estimated directly on the ROI ($MFG_L$) signal in the four conditions (Rest, ExtAtt, IntAtt, IntExtAtt). **Panel B** – Comparison between the PSD estimated directly on the ROI signal (blue lines, the same curves as in Panel A) and the PSD obtained from the AR model of the ROI signal using model order 30 (red lines). Values are in $(\mu A/mm^2)^2/Hz$.

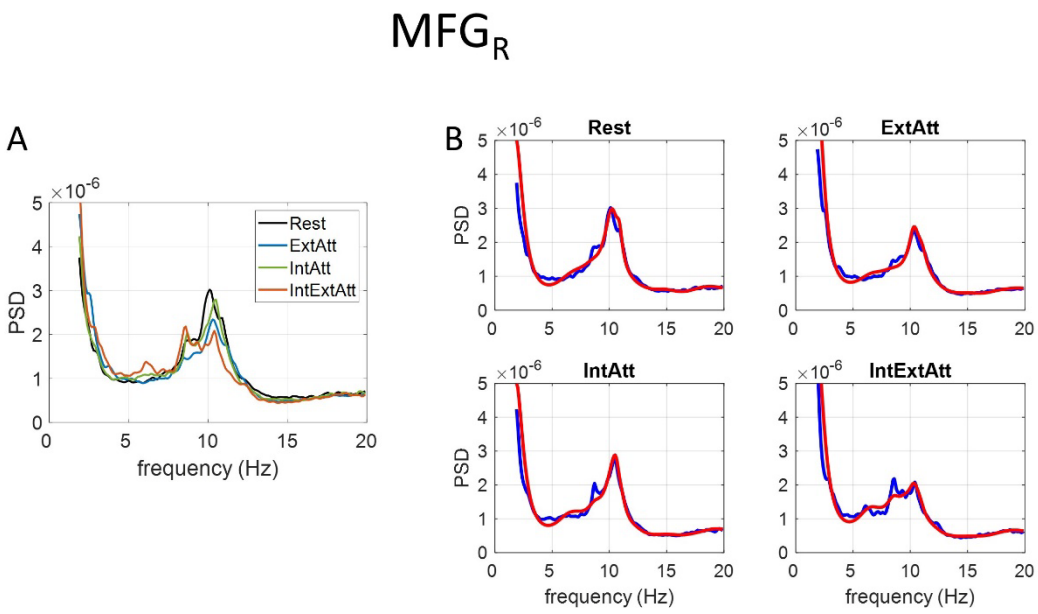


**Supplementary Figure 4**

**Supplementary Figure 4 - Panel A**: PSDs estimated directly on the ROI ($MFG_R$) signal in the four conditions (Rest, ExtAtt, IntAtt, IntExtAtt). **Panel B** – Comparison between the PSD estimated directly on the ROI signal (blue lines, the same curves as in Panel A) and the PSD obtained from the AR model of the ROI signal using model order 30 (red lines). Values are in $(\mu A/mm^2)^2/Hz$.

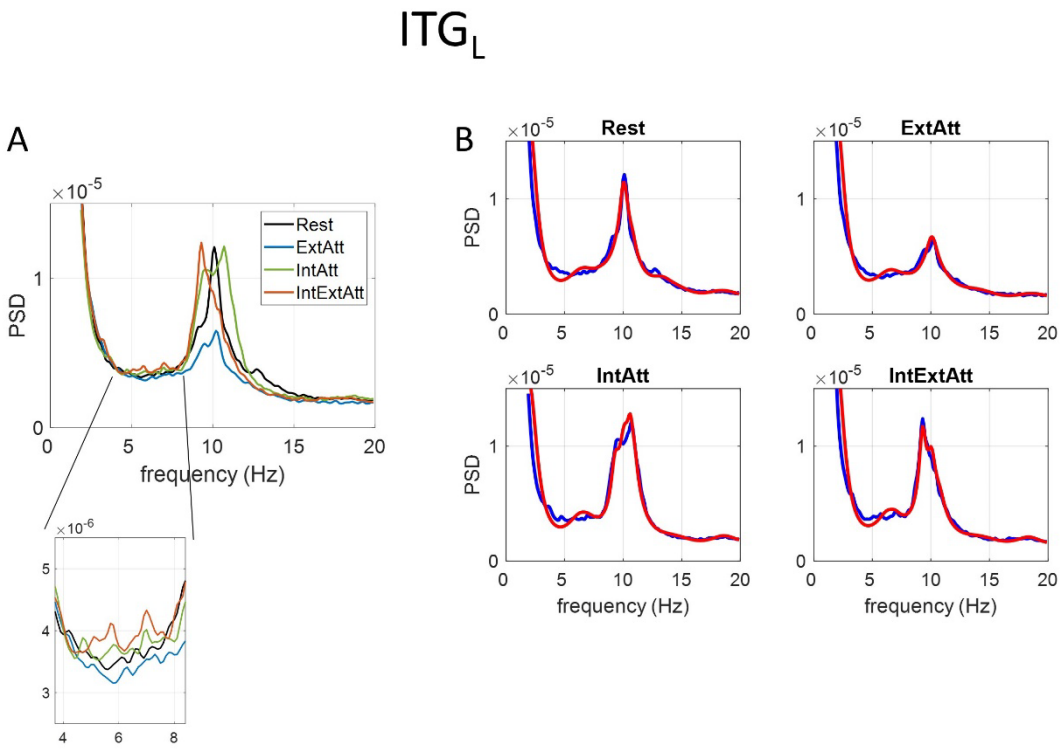


## Supplementary Figure 5

**Supplementary Figure 5 - Panel A**: PSDs estimated directly on the ROI ($ITG_L$) signal in the four conditions (Rest, ExtAtt, IntAtt, IntExtAtt). The zoom in focuses on the portion roughly corresponding to the theta band. **Panel B** – Comparison between the PSD estimated directly on the ROI signal (blue lines, the same curves as in Panel A) and the PSD obtained from the AR model of the ROI signal using model order 30 (red lines). Values are in $(\mu A/mm^2)^2/Hz$.

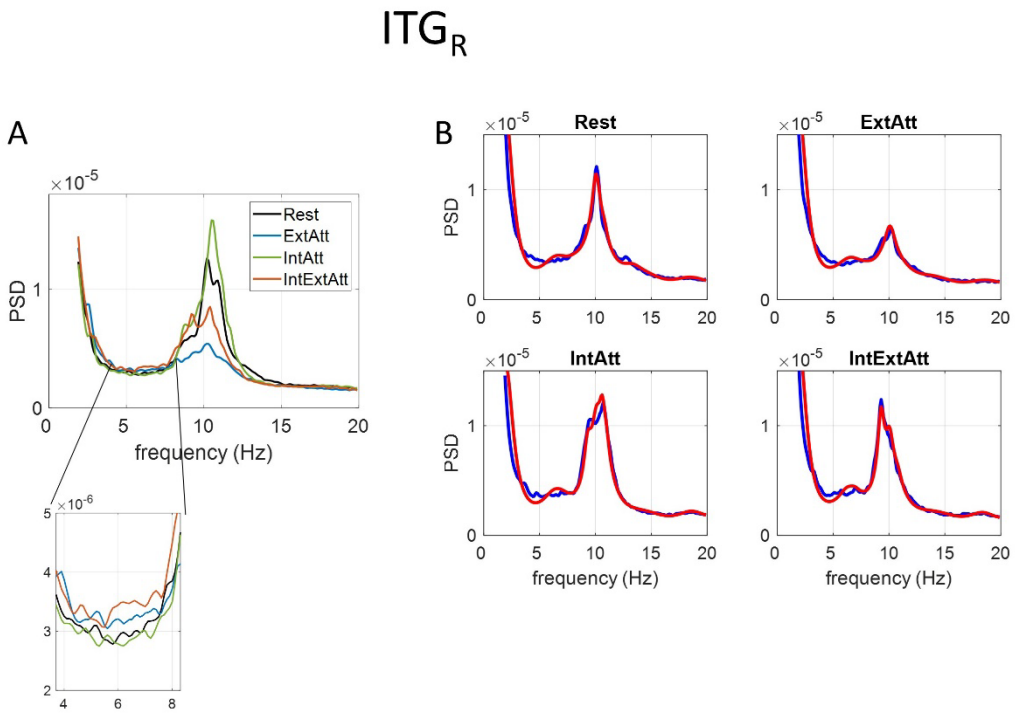


## Supplementary Figure 6

**Supplementary Figure 6 - Panel A**: PSDs estimated directly on the ROI ($ITG_R$) signal in the four conditions (Rest, ExtAtt, IntAtt, IntExtAtt). The zoom in focuses on the portion roughly corresponding to the theta band. **Panel B** – Comparison between the PSD estimated directly on the ROI signal (blue lines, the same curves as in Panel A) and the PSD obtained from the AR model of the ROI signal using model order 30 (red lines). Values are in $(\mu A/mm^2)^2/Hz$.

PCU

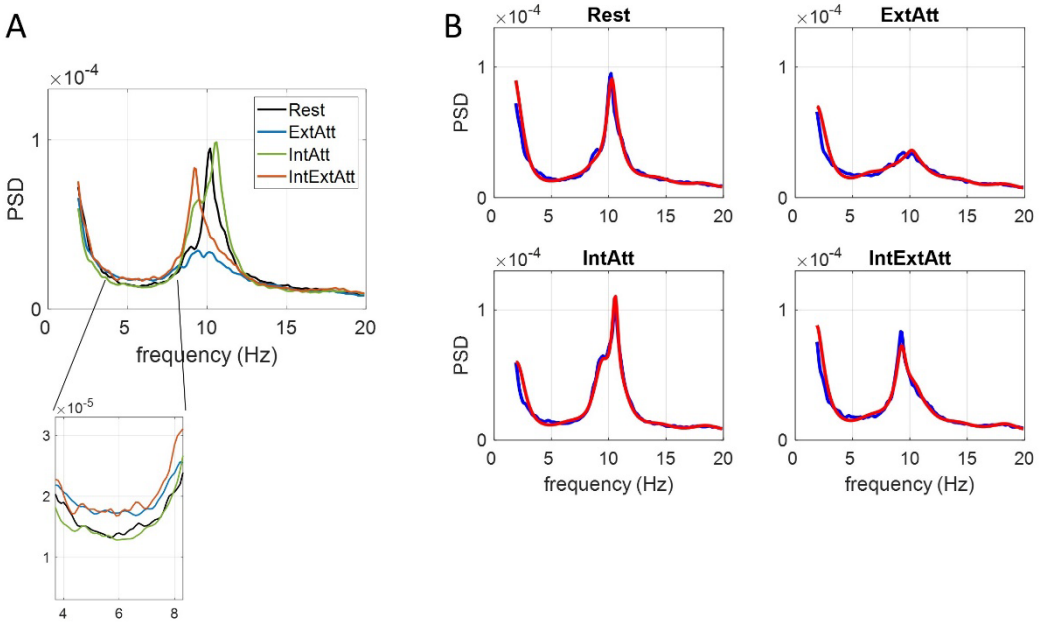


## Supplementary Figure 7

**Supplementary Figure 7 - Panel A**: PSDs estimated directly on the ROI (PCU) signal in the four conditions (Rest, ExtAtt, IntAtt, IntExtAtt). The zoom in focuses on the portion roughly corresponding to the theta band. **Panel B** – Comparison between the PSD estimated directly on the ROI signal (blue lines, the same curves as in Panel A) and the PSD obtained from the AR model of the ROI signal using model order 30 (red lines). Values are in $(\mu A/mm^2)^2/Hz$.

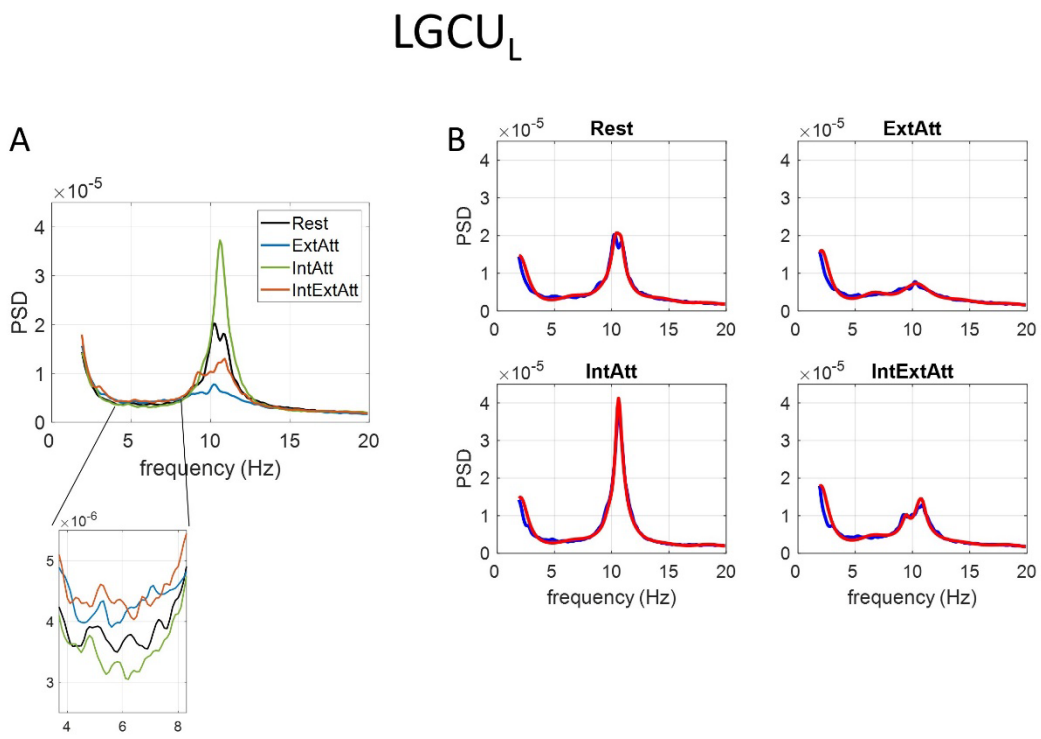


## Supplementary Figure 8

**Supplementary Figure 8- Panel A**: PSDs estimated directly on the actual ROI ($LGCU_L$) signal in the four conditions (Rest, ExtAtt, IntAtt, IntExtAtt). The zoom in focuses on the portion roughly corresponding to the theta band. **Panel B** – Comparison between the PSD estimated directly on the ROI signal (blue lines, the same curves as in Panel A) and the PSD obtained from the AR model of the ROI signal using model order 30 (red lines). Values are in $(\mu A/mm^2)^2/Hz$.

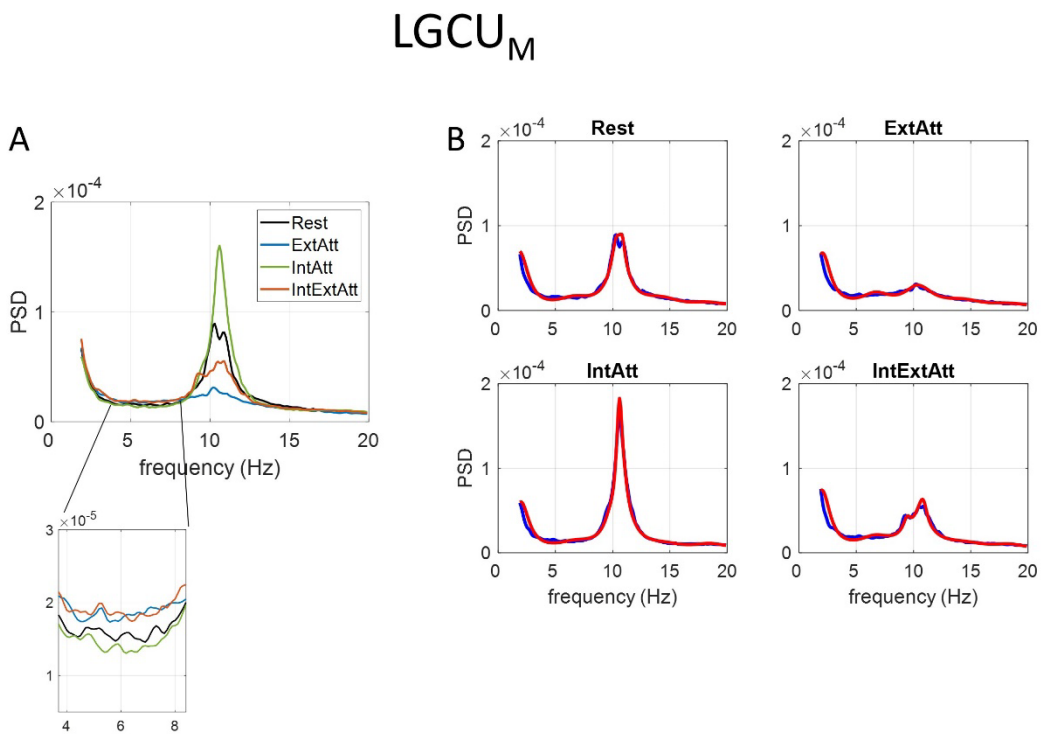


## Supplementary Figure 9

**Supplementary Figure 9 - Panel A**: PSDs estimated directly on the ROI ($(LGCU_M)$ signal in the four conditions (Rest, ExtAtt, IntAtt, IntExtAtt). The zoom in focuses on the portion roughly corresponding to the theta band. **Panel B** – Comparison between the PSD estimated directly on the ROI signal (blue lines, the same curves as in Panel A) and the PSD obtained from the AR model of the ROI signal using model order 30 (red lines). Values are in $(\mu A/mm^2)^2/Hz$.

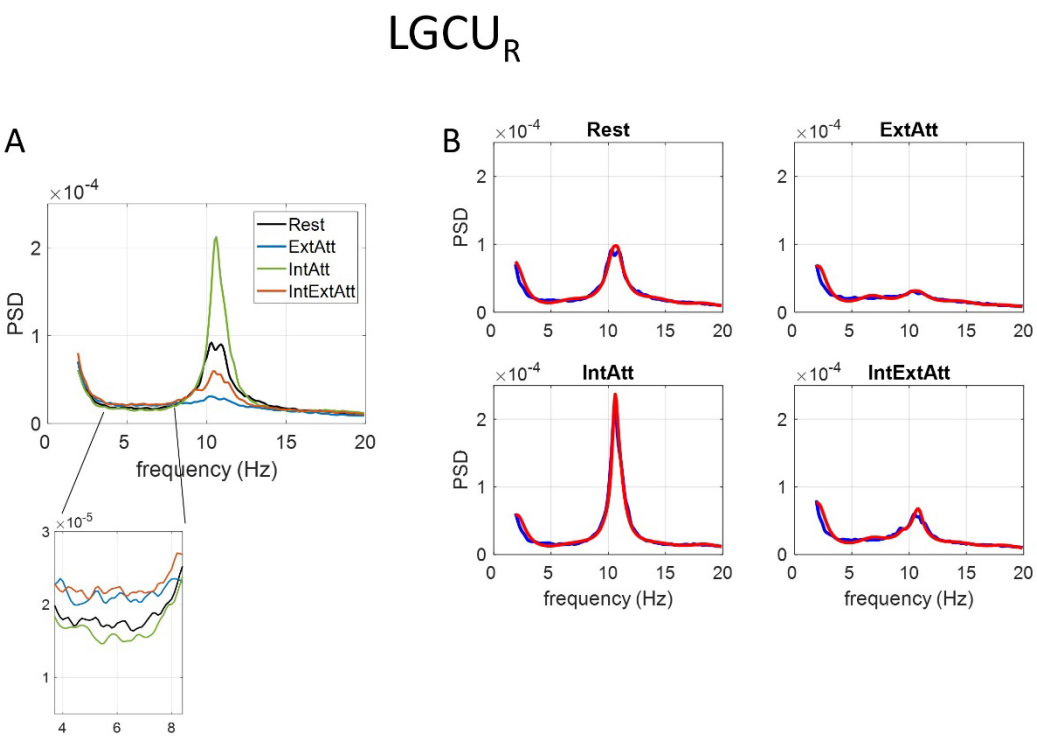


## Supplementary Figure 10

**Supplementary Figure 10 - Panel A**: PSDs estimated directly on the ROI (($LGCU_R$) signal in the four conditions (Rest, ExtAtt, IntAtt, IntExtAtt). The zoom in focuses on the portion roughly corresponding to the theta band. **Panel B** – Comparison between the PSD estimated directly on the ROI signal (blue lines, the same curves as in Panel A) and the PSD obtained from the AR model of the ROI signal using model order 30 (red lines). Values are in $(\mu A/mm^2)^2/Hz$.